



VICTORIA UNIVERSITY
MELBOURNE AUSTRALIA

Mitigation of Reverse Intermodulation Products at Colocated Base Stations

This is the Accepted version of the following publication

Ahmed, Shabbir and Faulkner, Michael (2012) Mitigation of Reverse Intermodulation Products at Colocated Base Stations. *IEEE Transactions on Circuits and Systems Part 1: Regular Papers*, 60 (6). pp. 1608-1620. ISSN 1549-8328

The publisher's official version can be found at
<http://ieeexplore.ieee.org/xpl/articleDetails.jsp?arnumber=6365774>
Note that access to this version may require subscription.

Downloaded from VU Research Repository <https://vuir.vu.edu.au/22815/>

Mitigation of Reverse Intermodulation Products at Colocated Base Stations

Shabbir Ahmed, *Student Member, IEEE*, and Mike Faulkner, *Member, IEEE*

Abstract—In a colocated setting, large jamming signals from one transmitter can radiate into the antenna system of a second transmitter. The signals enter the second transmitter in the reverse direction and mix in the output stage of its power amplifier to produce intermodulation products. These ‘reverse’ intermodulation products get radiated from the antenna system and may fall on the victim receiver’s desired channel. The paper proposes an architecture that regenerates an estimate of the reverse intermodulation products using the fundamental jammer components and mitigates them in a baseband postdistortion cancellation circuit. A novel multiple-front-end receiver architecture is developed to overcome the high sample rate requirements if the jammers are well out of band. However, this leads to a frequency offset problem in the regenerated distortion estimate. Signal correlation is used to align the frequency, phase and amplitude of the distortion estimate with the interfering reverse intermodulation product. Simulations and theoretical analysis show the output signal-to-interference ratio (SIR) of the system is independent of the input SIR but dependent on the equivalent number of uncorrelated samples in the averaging block. A hardware prototype demonstrated a 16dB reduction of the interfering reverse intermodulation product.

Index Terms—Intermodulation products, postdistortion cancellation, frequency offset correction, colocation, interference suppression, land mobile radio equipment, radio receivers, digital signal processing.

I. INTRODUCTION

COLOCATION of multiple transceivers of different wireless standards on one common site increases the potential for mutual interference due to the close proximity of antennas. The problem is well recognised in the Defence industry where different air/land/marine vehicles have to accommodate many radio frequency (RF) platforms in a small area [1] [2] [3]. Lately, the rapid growth of the wireless industry has led to the deployment of a large number of base stations. Thus, the availability of new green field sites has been exhausted and service providers are now forced to share a common site. Although, sharing a common site reduces maintenance, rental, logistics and other costs, it causes interference challenges that need to be addressed.

In a co-located setting, base-station receivers have to receive weak desired signals in the presence of strong transmit signals (also called jamming signals in this paper) from neighbouring base-station transmitters; resulting in desensitization and the formation of intermodulation (IM) products. There are two major sources of IM products that may fall in the desired receive channel of the victim receiver [4].

The first are the IM products produced when high powered jamming signals from the colocated transmitters mix

within the victim receiver’s front-end circuits (viz., low noise amplifier, mixer). The large jamming signal(s), regardless of their carrier frequencies, could also desensitize the receiver by forcing its circuits into saturation [5] [6]. Paper [7] addresses in detail such scenarios and proposes a feasible solution.

The second source of IM products are those radiated from the colocated transmitters themselves. In particular, the IM products that are generated when a high powered jamming signal from one transmitter radiates into the antenna system of a second transmitter and mixes in the output stage of its power amplifier (PA). These distortions are more precisely termed as ‘reverse’ IM products because of the manner in which they are produced and are specific to colocated scenarios. They may fall directly in the receive channel of a colocated victim receiver and cause interference. Further, the jammers need not necessarily be in-band, they could be out-of-band and still produce distortions within the victim receiver’s desired channel. In the case of out-of-band jammers both odd-order and even-order IM products could be of concern. Our paper here focuses on the elimination of these reverse IM products.

The European Telecommunications Standards Institute (ETSI) standard [8] limits transmitter spurious output levels to $-36\text{dBm}/0.1\text{MHz}$ below 1GHz, which is still too high to protect co-sited receivers. If co-sited receivers are present then there is a further reduction in the allowable spurious levels to -96dBm in the receive bands of other UMTS receivers on the same site. Unfortunately, it is not always possible to predict what future systems will be added to the site and so avoid the retrospective application of additional low insertion loss transmit filters, isolators or antenna placement strategies. The problem is even more difficult with the latest frequency agile cognitive technologies. It is the expense of retrofitting these systems we are trying to avoid.

Netcom [9] proposed an integrated frequency agile band-pass filter at the transmitter output to reject reverse signals entering the PA as well as stop any IM products produced from being transmitted. However, frequency agile high- Q filters with low insertion loss would be required to sufficiently attenuate the large transmitter signals, which, in some cases, have output powers of $+47\text{dBm}$ (50W) [10]; a difficult and costly challenge. The scheme was targeted at defense applications but is commercially unfeasible for many wireless service providers.

Another transmitter-end solution is proposed by the proponents of [11]. A direct feed from one jammer is gain-phase adjusted and coupled into the output of a second colocated jammer such that it is 180° out of phase to the corresponding jamming signal that radiates in through the antenna system. The method provides very good cancellation (35dB) but adds

The authors are with the School of Engineering and Science, Victoria University, PO Box 14428, Melbourne, Victoria 8001, Australia (email: Shabbir.Ahmed@live.vu.edu.au, Mike.Faulkner@vu.edu.au).

TABLE I
RELATED IM DISTORTION MITIGATION SYSTEMS

Ref.	Cancellation Scheme	Mitigating	Analog / Digital	Comments / Issues	Cancellation
[18]	IM2 at Rx	Rx IM	Analog & Digital	DC-offset, noise, analog impairments	22dB
[19] [20]	Multi-IMs at Rx	Rx IM	Analog & Digital	DC-offset, noise, analog impairments	24dB
[21]	Multi-IMs at Rx	Rx IM	Digital	High ADC sampling rate	25dB
[7]	Jammer at Rx	Rx IM	Analog	Reference path noise	25dB
[11]	Jammer at Tx	Tx reverse IM	Analog	Insertion loss, direct feed between jamming transmitters	35dB
This paper	IM3 (extendable) at Rx	Tx reverse IM	Digital	Frequency offset, multiple receiver chains	16dB

insertion loss to the transmit path, and more importantly the victim receiver needs collaboration from the aggressor jammers for such transmit-end solutions. This is less likely in a multiple service provider scenario since it incurs further capital expenditures and the victim service provider is possibly a competitor. A solution is therefore required, that can be independently deployed by the victim receiver.

In [7], we used an adaptive cancellation system to reduce the jammers that hit the victim receiver front-end, thus, mitigating the formation of IM products. Likewise, authors of [3] removed them with tunable notch filters deployed at the victim receiver. However, removing the jammers at the victim receiver does not help mitigating the reverse IM products that are produced at the transmitter-end.

An alternate approach is to allow the distortion to occur and then cancel it at the victim receiver by regenerating an estimate of the distortion using the fundamental jammers. The concept, known as postdistortion, is the inverse of predistortion which is well researched and used in PA linearization. Predistortion systems can use either analog circuits or digital polynomial functions [12]- [17]. Similar circuits can be used to linearize receivers. The authors [18] and [19] used analog circuits to synthesize a distortion estimate for use in a digital adaptive postdistortion cancellation technique. Analogue squaring and cubing circuits often have inherent complexities such as direct feed-through, DC-offsets, temperature drifts and poor noise performance. On the other hand, digital polynomial functions have none of these problems; they are perfect (to within the quantization noise limit). Authors of [21] performed both distortion regeneration and distortion cancellation in the digital domain. The distortion corrupted desired signal along with the jammers are received in the RF front-end and downconverted to digital baseband. However, the demonstrated system is bandlimited by the ADC's sampling rate and is unable to mitigate distortions produced by out-of-band jammers unless extremely large sampling rates are employed, making it both expensive and power hungry. The authors suggested the use of two parallel front-ends and ADC stages as a potential solution; one for the desired signal band and the other for blocker(s). This reduces the ADC resolution and sampling rate requirements. No further details were given.

The above postdistortion canceling schemes that target distortions generated within the victim receiver are summarized in Table I (first four entries). The set of jammers that generate the distortion estimate in the regeneration circuits are exactly the same as those that generate the distortion products in

the receiver circuits. However, the dominant jammers causing the reverse IM products at the transmitter might not be the dominant jammers at the victim receiver. This sets the need for jammer selectivity for the regeneration circuits at the receiver. A full digital solution, similar to that of [21], would give the required flexibility for jammer selection, but the requirements of extremely high ADC sampling rates and processing power need to be addressed.

In this paper, we take advantage of the growing availability of low cost, wide-band software defined radios (SDRs) [22] [23] to extend the two-receiver solution suggested by [21] into a multi-receiver solution. We propose a novel postdistortion cancellation system using multiple SDR front-ends with reduced ADC sampling rate. As seen in Fig. 1, the primary SDR front-end (Rx0) receives the corrupt desired signal and converts it to digital baseband (y). The auxiliary SDR front-ends (Rx1, Rx2,...) are each tuned to a jamming signal that contributes to the interfering reverse IM distortion. These signals are also converted to digital baseband where they are described by their complex envelope representation (a, b, \dots). The fundamental jamming signals are processed in a nonlinear function to produce an estimate \hat{u} of the required reverse distortion product u . This is then subtracted from the primary received signal after appropriate gain and phase scaling. This effectively eases the spurious requirements for transmitter reverse intermodulation.

The structure of the nonlinear function depends on the distortion source, which can be from within the victim receiver

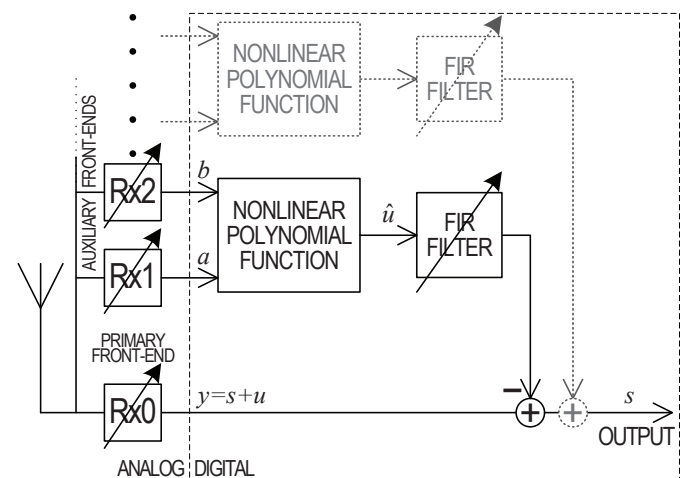


Fig. 1. Proposed reverse IM postdistortion solution.

or from outside such as from passive IM distortion from poor connections or reverse intermodulation as discussed here. Even and odd order harmonics as well as multi-signal IM products can be synthesised using a polynomial function.

The scheme relies on the exact match in amplitude, phase and frequency of the distortion estimate \hat{u} with the distortion u in the received signal y . This can only be achieved if the frequency of the jamming signals are known. In practice, this assumption might not be valid, and even if the frequencies are known (e.g., from database look-up), component tolerances, aging and temperature drifts in the transceiver reference crystals produce unknown frequency offsets. If the jammer modulation is known the offset can be estimated using coherent detection. For example, carrier frequency offset [24] correction using pilots, cyclic prefix and signal statistics is well known for OFDM signals [25]- [27].

The solution proposed here does not require knowledge of these offsets or knowledge of the jamming signals' modulation. No spectral or time domain information about the jammers is assumed. However what is assumed, is the jammers are large and can be identified by a scanning receiver using simple energy detection. The frequency estimates are therefore very coarse and must be corrected as part of the distortion synthesis process. A novel two part frequency correction technique is described in this paper. It involves a combination of FFT and signal correlation to correct the frequency offset in the synthesized distortion.

Section II discusses a colocated base station model and the reverse IM products that cause interference. Section III describes the novel distortion synthesis technique with frequency correction and the proposed postdistortion cancellation architecture. Section IV characterizes the cancellation system using simulations and mathematical analysis. Section V presents a practical prototype of the cancellation system, measurements and results. Finally, section VI is the conclusion.

II. REVERSE INTERMODULATION PRODUCTS

A model of three colocated base stations along with a remote terminal is shown in Fig. 2. Terminal D transmits the desired signal $s_r^D(t)$ ¹ over channel gain $h_d(t)$ to base station receiver RX. The spectrum of the output at terminal D shows the desired signal $s_r^D(t)$ at frequency channel f_d .

A high powered signal $b_r^B(t)$ from jammer B propagates through a channel gain of h_{ba} into the colocated power amplifier of jammer A and produces reverse third-order intermodulation (IM3) products $u_r^A(t)$ and $v_r^A(t)$; with $u_r^A(t)$ at f_u , overlapping receiver RX's desired channel frequency f_d , and $v_r^A(t)$ is at frequency f_v , given as follows,

$$f_u = 2f_a - f_b \quad (1)$$

$$f_v = 2f_b - f_a \quad (2)$$

where f_a and f_b are the transmit frequencies of $a_r^A(t)$ and $b_r^B(t)$ respectively. The IM3 products $u_r^A(t)$ and $v_r^A(t)$ are

¹Radio frequency signals have the subscript 'r'. $s_r^D(t) = \text{Re} [s^D(t)e^{j2\pi f_d t}]$, where $s^D(t)$ is the complex envelope.

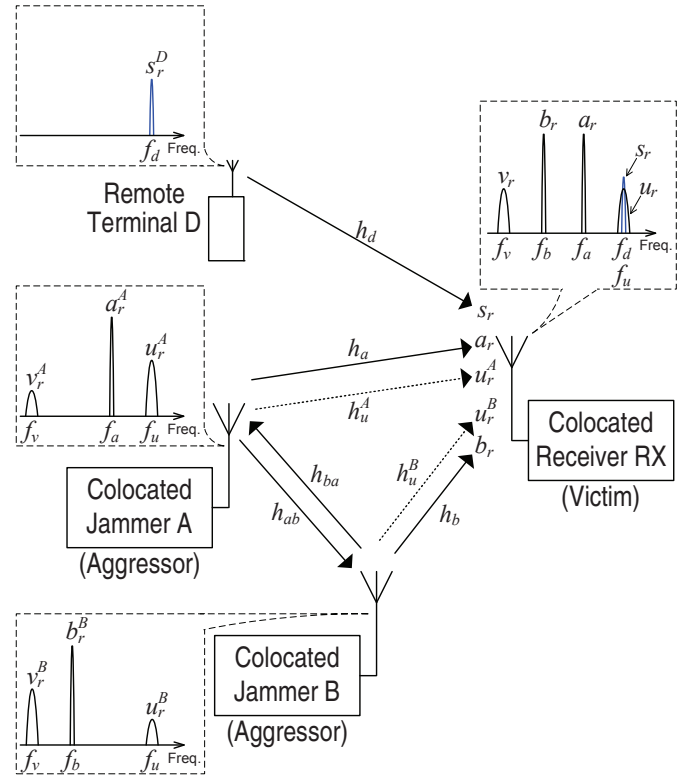


Fig. 2. Colocated base station transceivers.

radiated from jammer A along with its own transmission. Spectrum A shows the output at jammer A.

Similarly, signal $a_r^A(t)$ from jammer A propagates over a channel gain of h_{ab} to generate reverse IM3 products $u_r^B(t)$ and $v_r^B(t)$ at jammer B. Spectrum B shows the output at jammer B.

Spectrum RX shows the signals $v_r(t)$, $b_r(t)$, $a_r(t)$, $u_r(t)$ and $d_r(t)$ received at receiver RX after propagating through their respective channel gains. Reverse IM3 product $v_r(t)$ does not affect desired channel f_d and is not of concern.

Large transmit signals $a_r(t)$ and $b_r(t)$ could be of considerable concern if they exceed the dynamic range levels of receiver RX as discussed in [7]. However, in this paper, we consider them to be within receiver RX's dynamic range and so do not contribute to the distortions within the receiver's front-end.

Reverse IM3 product $u_r(t)$ falls directly on to the desired signal channel f_d and causes interference for receiver RX. The IM3 product $u_r(t)$ has two components $u_r^A(t)$ and $u_r^B(t)$ given by,

$$u_r(t) = \text{Re} [(h_u^A u^A(t) + h_u^B u^B(t)) e^{j2\pi f_u t}] \quad (3)$$

where h_u^A and h_u^B are the respective channel gains through which $u_r^A(t)$ and $u_r^B(t)$ propagate to receiver RX (Note: These gains are different from h_a and h_b because they are at different carrier frequencies); $u^A(t)$ and $u^B(t)$ are the complex envelopes.

The IM3 product $u_r^A(t)$ is linearly affected by the channel gain h_{ba} , its magnitude is given as follows,

$$|u^A(t)| = g_3^A |h_{ba}| |a^A(t)|^2 |b^B(t)| \quad (4)$$

where g_3^A is the cubic distortion coefficient of jammer A's power amplifier and is related to its output IP3 [6]. However, the magnitude of the IM3 product $u_r^B(t)$ depends on the square of the channel gain h_{ab} , as given below,

$$|u_r^B(t)| = g_3^B |h_{ab}|^2 |a^A(t)|^2 |b^B(t)| \quad (5)$$

where g_3^B is the cubic distortion coefficient of jammer B's power amplifier. If both transmitter amplifiers are similar then the distortion coefficients $g_3^A \sim g_3^B$. Thus, $u_r^B(t)$ is usually very small and is considered negligible throughout this paper.

A point to note, although the channel gain $h_d(t)$ is time varying, the other gains shown in Fig. 2, h_a , h_u^A , h_b , h_u^B , h_{ba} and h_{ab} are all considered to be quasi-static given the close proximities and fixed nature of the colocated antennas A, B and C.

III. PROPOSED ARCHITECTURE AND DIGITAL SIGNAL PROCESSING

The proposed architecture (Fig. 3) has an antenna feeding three SDR front-ends and a common DSP that synthesizes the interfering reverse IM3 product and removes it from the contaminated desired signal before the demodulator.

If the cancellation is to be effective the synthesized distortion must have the correct amplitude, phase, timing and frequency. In this work timing accuracy is obtained by using the same sampling clock for all three receivers. Frequency locking is obtained using a correction algorithm and gain-phase correction is obtained by adaptive adjustment.

The sample rates have to be reasonably high because of frequency offsets and the bandwidth expansion that occurs on the nonlinear jamming signals. For example, the distortion u_r has a bandwidth of twice the bandwidth of the a_r signal plus the bandwidth of the b_r signal. A large over sampling rate will handle most contingencies as well as give reasonable timing fidelity in the cancellation. Note, the sample rate is still much less than a single wideband receiver covering all jamming and desired signals.

The next subsections describe the major modules in the system.

A. Multiple Receivers

The victim receiver has multiple independently tuned RF front-ends. The primary receiver front-end Rx0 is tuned to receive at the desired signal frequency f_d . It receives the desired signal $s_r(t)$ along with the interfering reverse IM3 product $u_r(t)$. The received signal,

$$y_r(t) = s_r(t) + u_r(t) \quad (6)$$

where,

$$s_r(t) = \text{Re} [h_d(t)s^D(t)e^{j2\pi f_d t}] \quad (7)$$

with $s^D(t)$ being the complex envelope of $s_r^D(t)$, and,

$$u_r(t) = \text{Re} \left[g_3^A h_u^A h_{ba} \{b^B(t)\}^* \{a^A(t)\}^2 e^{j2\pi(2f_a - f_b)t} \right] \quad (8)$$

with $a^A(t)$ and $b^B(t)$ being the complex envelopes of $a_r^A(t)$ and $b_r^B(t)$ respectively and $\{b^B(t)\}^*$ is the conjugate of $b^B(t)$.

As discussed the non-linear IM3 products have expanded bandwidths and can cover many channels. The center frequency of $u_r(t)$ could therefore have a frequency offset Δf_u of more than one channel from f_d (i.e. $2f_a - f_b = f_d + \Delta f_u$) and still cause interference to $s_r(t)$. Thus, $u_r(t)$ could be rewritten and expressed as follows,

$$u_r(t) = \text{Re} \left[g_3^A h_u^A h_{ba} \{b^B(t)\}^* \{a^A(t)\}^2 e^{j2\pi(f_d + \Delta f_u)t} \right] \quad (9)$$

The complex envelope of the received signal $y_r(t)$ is $y(t)$ at receiver Rx0's operating frequency f_d . After sampling and analog-to-digital conversion the digital baseband signal is given by,

$$y_n = s_n + u_n \quad (10)$$

where s_n is the desired signal component,

$$s_n = h_{d,n} s_n^D \quad (11)$$

and u_n is the IM3 distortion component,

$$u_n = g_u \{b_n^B\}^* \{a_n^A\}^2 e^{j2\pi\Delta f_u n/f_s} \quad (12)$$

with $g_u = g_3^A h_u^A h_{ba}$, and f_s is the sampling frequency of the software defined radios.

The auxiliary receiver front-ends Rx1 and Rx2 scan for the out-of-band jammers $a_r(t)$ and $b_r(t)$ respectively. These jammers are the fundamental components of the interfering IM3 product $u_r(t)$ and can be used to digitally synthesize the IM3 product at baseband. A relatively simple energy detection technique could be used to scan for the high powered jammers, since, an exact lock onto their carrier frequencies is not necessary. As such, the carrier frequencies f'_a and f'_b of their respective receiver front-ends Rx1 and Rx2 are at certain frequency offsets Δf_a and Δf_b from the jammer frequencies f_a and f_b , given as follows,

$$f_a = f'_a + \Delta f_a \quad (13)$$

$$f_b = f'_b + \Delta f_b \quad (14)$$

The following are the received signals at Rx1 and Rx2 respectively in terms of the complex envelope components of the jammers,

$$a_r(t) = \text{Re} \left[h_a a^A(t) e^{j2\pi(f'_a + \Delta f_a)t} \right] \quad (15)$$

$$b_r(t) = \text{Re} \left[h_b b^B(t) e^{j2\pi(f'_b + \Delta f_b)t} \right] \quad (16)$$

which at digital baseband are as follows,

$$a_n = h_a a_n^A e^{j2\pi\Delta f_a n/f_s} \quad (17)$$

$$b_n = h_b b_n^B e^{j2\pi\Delta f_b n/f_s} \quad (18)$$

The aim is to use these baseband jammer components a_n and b_n to synthesize a duplicate of the received distortion u_n and remove it from y_n .

²Assumes that $u_r^B(t)$ is negligible compared to $u_r^A(t)$. If not, due to amplifier differences, then the two distortion terms must be added giving $g_u = g_3^A h_u^A h_{ba} + g_3^B h_u^B h_{ab}^2$.

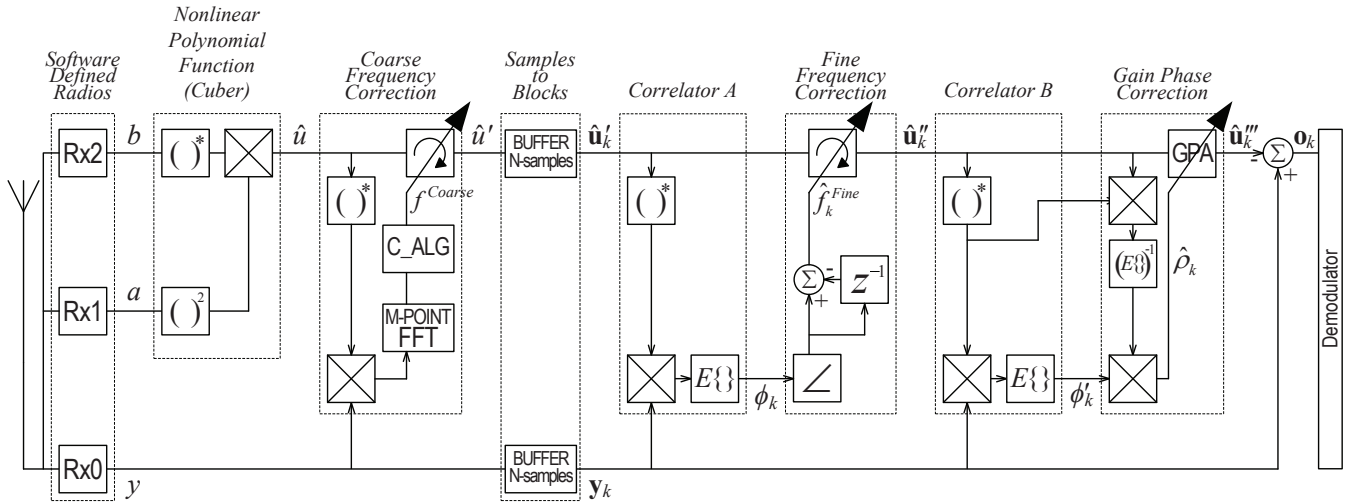


Fig. 3. Proposed DSP.

B. Nonlinear Polynomial Function: Cuber

The cuber module, as shown in Fig. 3, starts the synthesization process. It produces a sample of the required IM3 distortion by taking a_n and b_n as inputs, conjugating b_n and then multiplying with the square of a_n to give,

$$\hat{u}_n = b_n^* a_n^2 = g_{\hat{u}} \{b_n^B\}^* \{a_n^A\}^2 e^{j2\pi\Delta f_{\hat{u}} n/f_s} \quad (19)$$

where $g_{\hat{u}} = h_b^* h_a^2$ and $\Delta f_{\hat{u}} = (2\Delta f_a - \Delta f_b)$.

A comparison between Equations (12) and (19) shows that the synthesization process would further require a frequency offset Δf correction such that,

$$\Delta f_{\hat{u}} - \Delta f = \Delta f_u \quad (20)$$

and a gain-phase correction ρ such that,

$$\rho g_{\hat{u}} = g_u. \quad (21)$$

Hence, u_n is given as follows,

$$u_n = \rho \hat{u}_n e^{-j2\pi\Delta f n/f_s} \quad (22)$$

and y_n can be reformatted as,

$$y_n = s_n + \rho \hat{u}_n e^{-j2\pi\Delta f n/f_s}. \quad (23)$$

Further, the frequency tuning is a two part process. Where \hat{u} is rotated for a coarse correction of f^{Coarse} and then tracked in blocks and finely tuned by f^{Fine} , i.e.,

$$\Delta f = f^{Coarse} + f^{Fine}. \quad (24)$$

C. Coarse Frequency Correction

To do coarse frequency correction we must first find the distortion signal \hat{u} within y . To do this we use correlation.

$$\Phi = E \{ \hat{u}_n^* y_n \} \quad (25)$$

where $E\{\cdot\}$ is the expectation operator. Substituting for y_n from (23) gives

$$\Phi = E \{ \hat{u}_n^* s_n \} + E \left\{ \rho \hat{u}_n^* \hat{u}_n e^{-j2\pi\Delta f n/f_s} \right\}. \quad (26)$$

The first term is zero since \hat{u}_n is uncorrelated to s_n . The product of $\hat{u}_n^* \hat{u}_n$ is always real and averaging gives its power. However, the frequency offset term $e^{j2\pi\Delta f n/f_s}$ rotates the products and their average will tend to zero since most products would be balanced out with another product 180° out of phase. Thus, a second rotator is needed to reverse the frequency offset rotation prior to averaging. The FFT provides a bank of such rotators all rotating at different frequencies. It also provides the summation function for the averaging, and hence, it gives,

$$\Phi(l) = \sum_{n=0}^{M-1} \left\{ \hat{u}_n^* s_n + \rho \hat{u}_n^* \hat{u}_n e^{-j2\pi\Delta f n/f_s} \right\} e^{-j2\pi \frac{ln}{M}}, \quad l = 0, 1, \dots, M-1. \quad (27)$$

The correction algorithm C_ALG uses $\Phi(l)$ to find the highest power bin l_{max} in the M -point FFT, i.e., $l_{max} = \arg \max_l \Phi(l)$.

Which gives f^{Coarse} as follows,

$$f^{Coarse} = \delta_M l_{max} \quad (28)$$

where the frequency resolution is $\delta_M = f_s/M$. Large values of M are preferred in order to get an accurate frequency estimate as well as to minimize the noise contribution caused by the desired signal in the first term of (27).

Finally, the rotator in the coarse frequency correction module is set to correct \hat{u}_n by frequency f^{Coarse} such that,

$$\hat{u}'_n = \hat{u}_n e^{-j2\pi f^{Coarse} n/f_s}. \quad (29)$$

The correction is only accurate within half a bin size $\delta_M/2$. The small difference in rotation left between \hat{u}'_n and u_n in y_n is then adjusted by the fine frequency correction module. Generally, coarse frequency estimation is only performed once at switch ON.

D. Fine Frequency Correction

The stream of samples \hat{u}'_n and y_n is now buffered into blocks of N -samples, the k -th block is defined below,

$$\hat{\mathbf{u}}'_k = [\hat{u}'_{0,k} \ \hat{u}'_{1,k} \ \dots \ \hat{u}'_{(N-1),k}]^T \quad (30)$$

$$\mathbf{y}_k = [y_{0,k} \ y_{1,k} \ \dots \ y_{(N-1),k}]^T. \quad (31)$$

The blocks $\hat{\mathbf{u}}'_k$ and \mathbf{y}_k are then fed as inputs to correlator A.

Correlator A evaluates the correlation (ϕ_k) of $\hat{\mathbf{u}}'_k$ with \mathbf{y}_k ,

$$\phi_k = E\{\hat{u}'_{n,k}{}^* y_{n,k}\} \approx \left(\hat{\mathbf{u}}'^H_k \mathbf{y}_k \right) / N \quad (32)$$

and forwards it to the fine frequency correction module. The parameter of interest is the phase of ϕ_k ($\angle\phi_k$).

It is to be noted that \mathbf{y}_k has an IM3 distortion component \mathbf{u}_k and a desired signal component \mathbf{s}_k , i.e., $\mathbf{y}_k = \mathbf{u}_k + \mathbf{s}_k$. The aim is to align $\hat{\mathbf{u}}'_k$'s frequency rotation with \mathbf{u}_k . $E\{\hat{u}'_{n,k}{}^* y_{n,k}\}$ calculates the average of all the angle differences between each sample of $\hat{\mathbf{u}}'_k$ and \mathbf{u}_k . Hence, $\angle\phi_k$ holds the relative angle of the block $\hat{\mathbf{u}}'_k$ to \mathbf{u}_k . And $\angle\phi_{k-1}$ holds the relative angle of the previous block $\hat{\mathbf{u}}'_{k-1}$ to \mathbf{u}_{k-1} . The difference in the two angles,

$$\Delta\angle\phi = \angle\phi_k - \angle\phi_{k-1} \quad (33)$$

gives the extra phase rotation that $\hat{\mathbf{u}}'_k$ obtains due to the fine frequency offset over N -samples. The fine frequency estimate then becomes,

$$\hat{f}_k^{Fine} = \Delta\angle\phi f_s / 2\pi N. \quad (34)$$

The rotator uses \hat{f}_k^{Fine} to back rotate $\hat{\mathbf{u}}'_k$ with $\Delta\angle\phi/N$ radians/sample over the block.

$$\hat{u}''_{n,k} = \hat{u}'_{n,k} e^{-j2\pi\hat{f}_k^{Fine} n/f_s}. \quad (35)$$

This tunes $\hat{\mathbf{u}}''_k$ to the same frequency as \mathbf{u}_k in \mathbf{y}_k .

E. Gain-Phase Correction

We use Bussgang's theory [28] to identify the coefficient estimate $\hat{\rho}_k$ which is the amount of $\hat{\mathbf{u}}''_k$ in \mathbf{y}_k , i.e.,

$$\hat{\rho}_k = \frac{E\{\hat{u}''_{n,k}{}^* y_{n,k}\}}{E\{\hat{u}''_{n,k}{}^* \hat{u}''_{n,k}\}} \approx \frac{\left(\hat{\mathbf{u}}''^H_k \mathbf{y}_k \right)}{\left(\hat{\mathbf{u}}''^H_k \hat{\mathbf{u}}''_k \right)}. \quad (36)$$

Further, $\hat{\mathbf{u}}'''_k = \hat{\rho}_k \hat{\mathbf{u}}''_k$ is subtracted from \mathbf{y}_k to give us the desired signal \mathbf{s}_k which forms the input to the radio demodulator.

F. Desired Signal Demodulation

The received signal \mathbf{y}_k is essentially intact/unaltered until the distortion estimate $\hat{\mathbf{u}}'''_k$ gets subtracted at the input to the demodulator. Therefore, no modifications (e.g., frequency offset and gain-phase adjustment) are imposed on the desired signal \mathbf{s}_k . A standard receiver demodulator can be used. The demodulator would do the normal receiver functions of time synchronization, frequency synchronization, channel estimation and demodulation. Note, frequency synchronization here centers the desired signal modulation to DC. There is no relation between this and the frequency correction applied to the distortion estimate.

IV. SIMULATIONS AND ANALYSIS

In practice, a certain level of interference \mathbf{z}_k remain at the output of the system. Thus at the canceler output \mathbf{o}_k becomes,

$$\mathbf{o}_k = \mathbf{y}_k - \hat{\mathbf{u}}'''_k = \mathbf{s}_k + \mathbf{z}_k. \quad (37)$$

This section identifies the different sources of interference that cumulate to give \mathbf{z}_k at the output. The investigation works backward from the canceler output to isolate and identify each of the interference sources.

A. Buffer/Data Processing Block Size N

First, under investigation is the gain-phase correction module along with its correlator B that process data in blocks of N -samples; the preceding fine and coarse frequency correction modules are perfectly adjusted. Substituting for \mathbf{y}_k in equation (36), we have,

$$\hat{\rho}_k = \rho + \frac{E\{\hat{u}''_{n,k}{}^* s_{n,k}\}}{E\{\hat{u}''_{n,k}{}^* \hat{u}''_{n,k}\}}, \quad (38)$$

the latter term is zero, but, when the expectation takes the form of an average over N_s uncorrelated samples, the output approximates a normal distribution,

$$\hat{\rho}_k = \mathcal{N} \left\{ \rho, \frac{\sigma_s^2 \sigma_u^2}{N_s \sigma_u^4} \right\} \quad (39)$$

where the desired signal power $E\{|s_{n,k}|^2\} = \sigma_s^2$, and the distortion estimate power $E\{|\hat{u}_{n,k}|^2\} = \sigma_u^2$. Simplifying (39), we have,

$$\hat{\rho}_k = \mathcal{N} \left\{ \rho, \frac{\sigma_s^2}{N_s \sigma_u^2} \right\} \quad (40)$$

where the first term is the mean and the second term is the variance of a normal distribution. Since, the signals are over sampled we approximate $N_s = \eta N / OSR$ where OSR is the over-sampling rate of the desired signal and equal to $f_s/\text{bandwidth of } s$. The factor η is dependent on the modulation parameters of the signals a , b and s . We show in appendix A, $\eta = (3/2)^2$ when all three fundamental signals are Gaussian in nature and have a rectangular spectrum. Substituting $\hat{\mathbf{u}}'''_k$ in (37) with $\hat{\rho}_k \hat{\mathbf{u}}''_k$, we have,

$$\mathbf{o}_k = \mathcal{N} \left\{ \mathbf{s}_k, \frac{\sigma_s^2 \sigma_u^2}{N_s \sigma_u^2} \right\} \quad (41)$$

which is further simplified to give,

$$\mathbf{o}_k = \mathcal{N} \left\{ \mathbf{s}_k, \frac{\sigma_s^2}{N_s} \right\}. \quad (42)$$

Hence, output signal-to-interference ratio (SIR),

$$SIR_o = \sigma_s^2 / \frac{\sigma_s^2}{N_s} \quad (43)$$

which gives,

$$SIR_o = N_s. \quad (44)$$

We note, the SIR_o of \mathbf{o}_k is independent of the input SIR (SIR_y) of \mathbf{y}_k . The improvement in SIR is $(N_s - SIR_y)$ dB can be very large for heavily jammed signals, but can go negative if the input interference \mathbf{u}_k is weak! It is important therefore

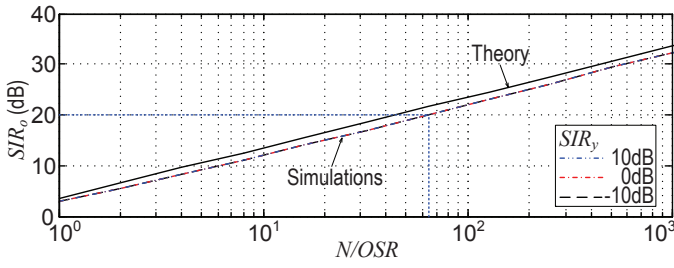


Fig. 4. SIR_o vs (N/OSR) . The figure shows SIR_o is independent of SIR_y .

to switch the canceling off if the SIR_y is better than N_s . The use of software radio architecture gives many control options for de-enabling the cancellation. For example, a blind method could consider the term $E\{|o_k|^2\} - E\{|y_k|^2\}$. A positive value would indicate the correction is doing more harm than benefit and should be terminated.

N_s sets the target SIR into the demodulator and is plotted in Fig. 4. Simulations verify the theoretical analysis and show a difference of about 1.5dB corresponding to the Gaussian assumption for the QPSK signals. Further, three SIR_y s (10dB, 0dB, -10dB) were taken, all produced the same curve, indicating the independence of SIR_o from SIR_y .

The simulations used QPSK modulated signals for the desired signal (s) and jammer signals (a and b). The symbols were Nyquist filtered with 50% excess bandwidth, and oversampled by $OSR = 64$.

In what follows, the analysis considers a block size $N = 2^{12} = 4096$ giving $N/OSR = 64$, and hence, $SIR_o = 20$ dB (as shown by the blue dotted lines in Fig. 4). This is sufficient for 16-QAM demodulation.

The analysis above assumes no frequency offset for the \hat{u}_k'' signal. A small frequency offset will add a linear phase component to \hat{u}_k'' . In the absence of the fine frequency correction block the signal,

$$\hat{u}_{n,k}''' = \hat{\rho} \hat{u}_{n,k}'' e^{j(-\theta/2 + \theta n/N)} \quad (45)$$

where the phase change over the block,

$$\theta = 2\pi f^{Fine} N / f_s. \quad (46)$$

After the final subtraction the error caused by the offset is given by $\rho \hat{u}_{n,k}'' - \hat{u}_{n,k}'''$, and can be approximated for small θ to give,

$$o_{n,k} = s_{n,k} + \rho \hat{u}_{n,k}'' - \hat{\rho}_k \hat{u}_{n,k}'' \left(1 + j \left(-\frac{\theta}{2} + \frac{\theta n}{N} \right) \right) \quad (47)$$

which includes the error contribution from $\hat{\rho}_k$ given by (40). The variance term is now

$$\sigma_z^2 \approx \frac{\sigma_s^2}{N_s} + \frac{1}{N} \sum_1^N \hat{\rho}_k^2 \hat{u}_n''^2 \left(-\frac{\theta}{2} + \frac{\theta n}{N} \right)^2 \quad (48)$$

expanding the brackets and considering only the dominant terms (since N is large) and approximating,

$$\sigma_z^2 \approx \frac{\sigma_s^2}{N_s} + \frac{\hat{\rho}_k^2 \sigma_u^2 \theta^2}{12} \quad (49)$$

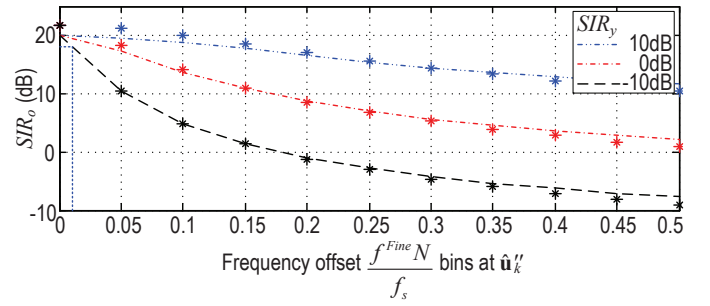


Fig. 5. The effect of frequency offset f^{Fine} on the output SIR. 1bin= f_s/N Hz. ‘*’s represent theoretical results.

where the first term is the variance from the error in ρ and the second term is the variance caused by the frequency offset. Substituting for θ and further approximating $\hat{\rho}_k^2 \sigma_u^2 \approx \sigma_s^2 / SIR_y$ we have,

$$o_k = \mathcal{N} \left\{ s_k, \frac{\sigma_s^2}{N_s} + \frac{(f^{Fine} N / f_s)^2 \pi^2 \sigma_s^2}{3 SIR_y} \right\}. \quad (50)$$

Fig. 5 shows how the output SIR is degraded with frequency offsets measured in bins (equivalent to an N -point FFT bin size of $f_{bin} = f_s/N$ Hz). The discrepancy between the simulations and theoretical is caused by the error in the first term as previously explained and the loss of the low angle assumption at larger f^{Fine} s. It is to be noted that SIR_o deteriorates with small frequency offsets, especially when y_k has a significant interference component u_k . Frequency offset should be less than 0.01 bins (i.e., $f^{Fine} < 0.01 f_s/N$ Hz), if $SIR_y = -10$ dB, and the implementation loss is to be restricted to less than 2dB (as shown by the blue dotted lines in Fig. 5). This is the goal of frequency correction discussed next.

B. Coarse Frequency Correction

The fine frequency correction module requires the residual frequency offset to be within ± 0.5 bins, therefore a good target for the coarse frequency correction module is to reduce the residual frequency offset f^{Fine} on \hat{u}_k' to within 0.25 bins (i.e. $f^{Fine} \leq 0.25 f_s/N$ Hz). Hence, from (24) we have,

$$\Delta f - 0.25 f_s/N \leq f^{Coarse} \leq \Delta f + 0.25 f_s/N. \quad (51)$$

As discussed earlier in section III-C, the coarse correction module is accurate within 0.5 bins of the M -point FFT (equivalent to $0.5 f_s/M$ Hz). Hence, evaluating $0.25 f_s/N = 0.5 f_s/M$ gives the required number of FFT points on the coarse correction module $M = 2N$ (8192).

However, the M -point FFT can be forced into error by the presence of s in y . In the worst case scenario where the frequency offset is on a bin boundary, the target residual offset ($f^{Fine} \leq 0.25 f_s/N$ Hz) is achieved if the highest power bin l_{max} is one of the two bins on either side of the offset bin boundary. The solid line (blue) Fig. 6 shows the probability of l_{max} being one of the two bins for increasing powers of s (i.e. increasing SIR_y). At $SIR_y = 10$ dB, the probability of f^{Coarse} being within range (51) is 97%. But values of SIR_y

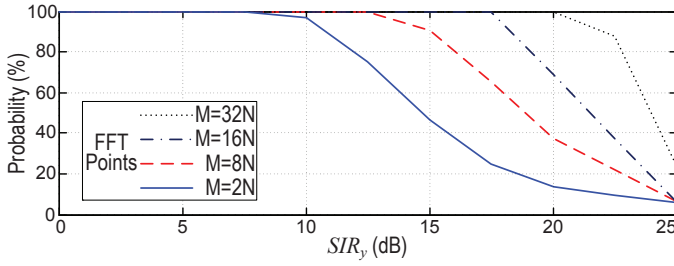


Fig. 6. Probability of acceptable coarse frequency correction ($\Delta f - 0.25f_s/N \leq f^{Coarse} \leq \Delta f + 0.25f_s/N$) for $M = 2N$, $M = 8N$, $M = 16N$ and $M = 32N$.

greater than 10dB force l_{max} outside the two expected bins and the probability falls exponentially.

The performance at higher SIR_y s can be improved by increasing the number of FFT points M . This reduces the FFT bin sizes and its susceptibility to noise. It also increases the number of frequency bins that result in acceptable coarse correction. For example, a $M = 8N$ -point FFT results in $0.125f_s/N$ Hz bin sizes and l_{max} could be any one of 4 bins (two on either side of the offset bin boundary). Fig. 6 further illustrates the probability of f^{Coarse} being within range (51) for $M = 8N$, $M = 16N$ and $M = 32N$.

C. Fine Frequency Correction

The fine frequency correction module removes any remaining offsets after the initial coarse correction stage. The module is designed to operate within offsets of ± 0.5 bins (i.e., $f^{Fine} < |0.5f_s/N|$ Hz). There are two factors that affect the accuracy of the estimate \hat{f}_k^{Fine} , a)

- 1) the level of desired signal s_k in \mathbf{y}_k that acts as interference to the estimation process, and
- 2) the absolute value of frequency offset f^{Fine} on the input signal $\hat{\mathbf{u}}'_k$.

Expanding (32) by splitting y into its signal and distortion components and then using equation (22) and (29), gives,

$$\phi_k = \frac{1}{N} \sum_{n=1}^N s_{n,k} \hat{u}'_{n,k} + \frac{1}{N} \sum_{n=1}^N \rho \hat{u}_{n,k}^* \hat{u}_{n,k} e^{-j(\psi_k - \frac{\theta}{2} + \frac{\theta n}{N})}. \quad (52)$$

The linear phase shift is caused by the residual frequency offset f^{Fine} , and ψ_k is the mean phase offset of the block. The mean $\bar{\phi}_k \approx \rho \sigma_u^2 e^{-j\psi_k}$ comes from the second term, and is accurate when θ is small. The variance of the first term is $\sigma_{\phi_{k,1}}^2 = \sigma_s^2 \sigma_u^2 / N_s$. This variance is circularly symmetric and so the contribution to the phase error is a half of this value. The variance of the phase due to the first term is therefore,

$$\sigma_{\angle\phi_{k,1}}^2 = \frac{1}{2} \frac{\sigma_s^2 \sigma_u^2}{\rho^2 \sigma_u^4 N_s} = \frac{SIR_y}{2N_s}. \quad (53)$$

After the angles have been subtracted (i.e., $\Delta\angle\phi = \angle\phi_k - \angle\phi_{k-1}$), the fine frequency estimate \hat{f}_k^{Fine} is obtained from (34). The variance \hat{f}_k^{Fine} due to the first term in (52) becomes,

$$\sigma_{\hat{f}_{k,1}^{Fine}}^2 = \frac{SIR_y}{4\pi^2 N_s} \left(\frac{f_s}{N} \right)^2. \quad (54)$$

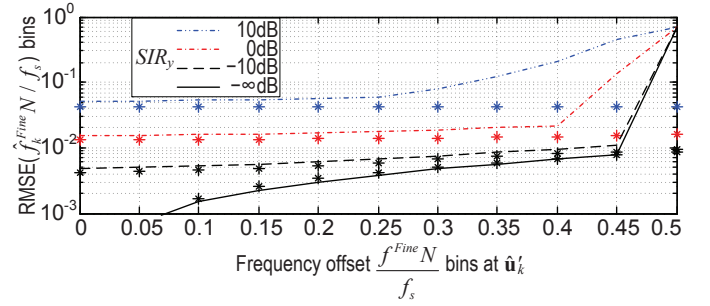


Fig. 7. Performance with feedforward fine frequency correction. '*'s represent theoretical results.

The second term of (52) contributes an additional variance when $f^{Fine} \neq 0$ resulting in a linear phase shift θ over the block. This makes the phase of ϕ_k dependent on the amplitudes of the individual $\hat{u}'_{n,k}$ samples. The variance of \hat{f}_k^{Fine} due to frequency offset is derived in the appendix B and the overall estimate \hat{f}_k^{Fine} becomes,

$$\hat{f}_k^{Fine} = \mathcal{N} \left\{ f^{Fine}, \frac{SIR_y}{4\pi^2 N_s} \left(\frac{f_s}{N} \right)^2 + \frac{(f^{Fine})^2}{24N_s} \right\}. \quad (55)$$

Fig. 7 shows the root mean square error of \hat{f}_k^{Fine} (i.e., $\text{RMSE}(\hat{f}_k^{Fine}) = \sqrt{E\{(\hat{f}_k^{Fine} - f^{Fine})^2\}}$) as a function of the actual frequency offset f^{Fine} . The solid black line represents an input \mathbf{y}_k without any s_k (i.e. $\mathbf{y}_k = \mathbf{u}_k$ and $SIR_y = 0$). The increase in $\text{RMSE}(\hat{f}_k^{Fine})$ with frequency offset is from the second term only. When $SIR_y \neq 0$ the minimum $\text{RMSE}(\hat{f}_k^{Fine})$ level is set by the first term of (52). There is good agreement between simulations and theory for frequency offsets below 0.25 bins (i.e., $f^{Fine} < 0.25f_s/N$ Hz). When the frequency offset f^{Fine} goes beyond 0.5 bins ($0.5f_s/N$ Hz) the phase difference $\angle\phi_k - \angle\phi_{k-1}$ crosses π and the estimate \hat{f}_k^{Fine} jumps from 0.5 bins to -0.5 bins, a catastrophic situation. In the diagram the variance in the phase $\angle\phi_k$ causes \hat{f}_k^{Fine} to jump prematurely at lower frequency offsets, indicated by the steep rise in RMSE. This scheme will only work if the residual frequency offset f^{Fine} after the coarse correction is $\ll 0.5$ bins (i.e., $f^{Fine} \ll 0.5f_s/N$ Hz).

D. Improved Feedback Fine Frequency Correction

An improved architecture with a feedback fine frequency correction is proposed to reduce the probability of exceeding the discontinuity at $f^{Fine} = 0.5$ bins ($0.5f_s/N$ Hz) as well as reduce the averaging error caused by frequency offsets in (55). We correct the frequency offset prior to estimating $\angle\phi_k$, as shown in Fig. 8,

$$\hat{u}_{n,k}'' = \hat{u}_{n,k}' e^{-j2\pi \hat{f}_{k-1}^{Fine} n / f_s}. \quad (56)$$

The correlator C now only has to calculate the change in f^{Fine} between blocks. An integrator holds the total estimate \hat{f}_k^{Fine} ,

$$\hat{f}_k^{Fine} = \hat{f}_{k-1}^{Fine} + \Delta\angle\phi f_s / 2\pi N. \quad (57)$$

The scheme relies on any drift in frequency offset being slow. However, drifts that take the frequency offset beyond 0.5

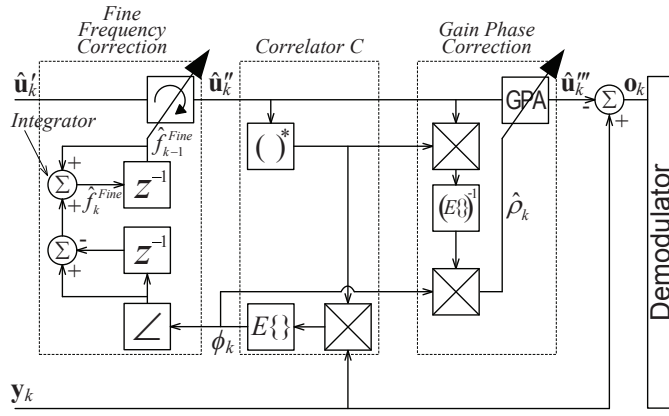


Fig. 8. Proposed feedback fine frequency correction.

bins ($0.5f_s/N$ Hz) can now be tracked. The key requirement is that the change in frequency per block must be $\ll 0.5$ bins. Fig. 9 shows the improved performance with respect to f^{Fine} , the contribution from the second term in (55) is nearly eliminated. Fig. 10 compares the two schemes tracking a frequency drift of magnitude 10^{-5} bins per sample ($10^{-5}f_s^2/N$ Hz/sec). The feedforward scheme fails to track the frequency offset once it drifts beyond 0.5 bins (in line with previous observations in Fig. 7). This is because the feedforward scheme calculates the total frequency offset of \hat{u}'_k relative to u_k in each block stage. In contrast, the feedback scheme continues to track without any failures, since it only estimates the extra frequency offset that the current block has after correcting it with \hat{f}_{k-1}^{Fine} (which is the total tracked frequency offset at the previous block). However, the feedback design of the scheme makes \hat{f}_k^{Fine} to fall short of tracking the exact offset, because the offset keeps increasing with every sample; as demonstrated in the figure, the feedback scheme's tracking runs below the ideal tracking line.

Finally, it is to be noted that the feedback scheme can only track frequency drifts when it starts with small frequency offsets less than 0.5 bins ($0.5f_s/N$ Hz) depending on SIR_y . As observed earlier in Fig. 9, it can fail to track when starting with frequency offsets that are too high (e.g., 0.43 bins for $SIR_y = 10$ dB).

V. PRACTICAL MEASUREMENTS

In this section, a practical setup in accordance to Fig. 2 is used to demonstrate that two out-of-band jammers at

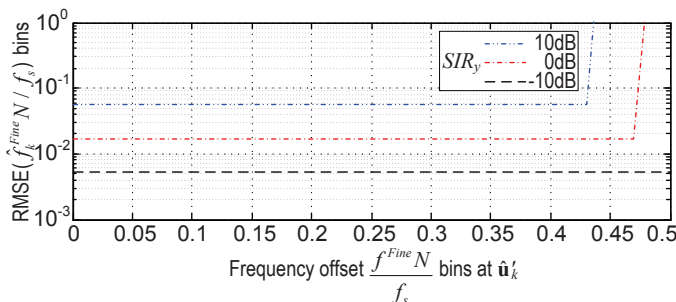
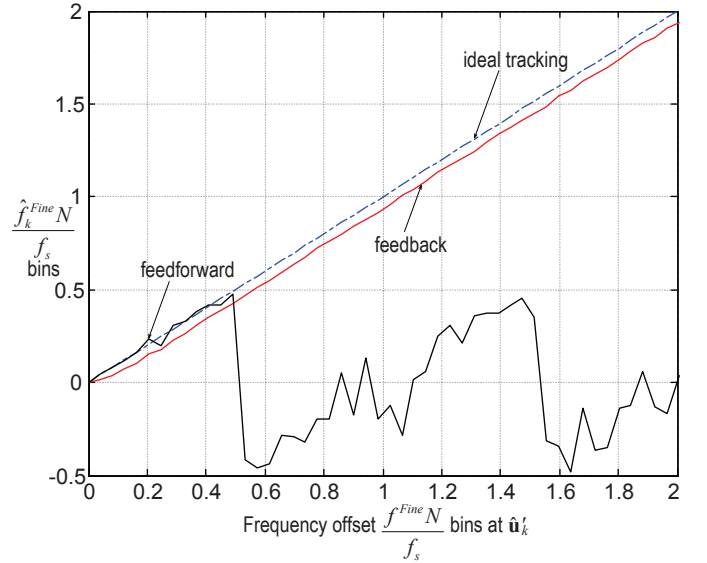


Fig. 9. Performance with feedback fine frequency correction.


 Fig. 10. Frequency drift tracking by \hat{f}_k^{Fine} .

a colocated setting generate reverse IM3 products causing major interference for the victim receiver. Further, a practical implementation of our proposed receiver architecture is demonstrated using Universal Software Radio Peripherals (USRPs) [22] as SDR front-ends. The signals are data-logged and processed in MATLAB.

Fig. 11 shows the two jammer antennas (A and B) colocated at close proximity to one another. Each jammer is a signal generator, QPSK modulated with an USRP and amplified by a power amplifier (Mini-Circuits ZHL-42W [29]), trans-

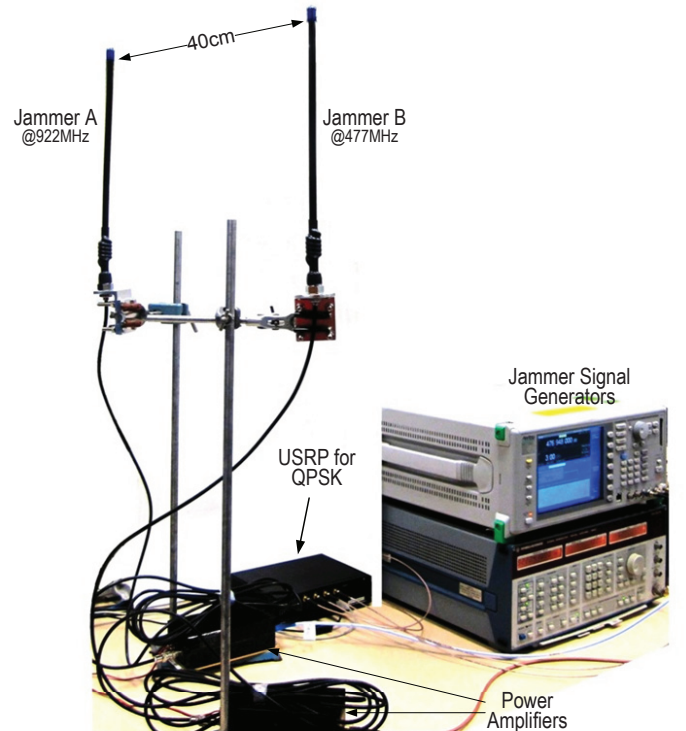


Fig. 11. Colocated transmitters generating reverse IM3 products.

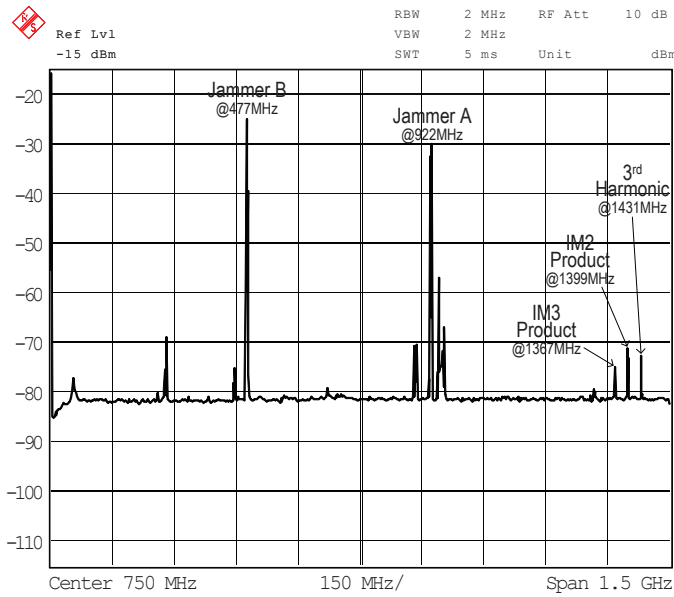


Fig. 12. Frequency spectrum of the jammers and distortions at RX's antenna.

mitting with an omni-directional dipole antenna. A small separation of 40cm is required to generate a considerable reverse IM3 product at the low transmitting powers in the laboratory setting. Jammer A transmits a 0.5W signal at 922MHz and jammer B transmits a 1W signal at 477MHz, this propagates into the power amplifier of jammer A and produces a reverse IM3 product at 1367MHz. Fig. 12 shows the frequency spectrum at the victim receiver RX's antenna. Adjacent to the 1367MHz reverse IM3, the spectrum shows the 1399MHz (922MHz+477MHz) reverse second-order intermodulation (IM2) product and the 1431MHz (3x477MHz) third harmonic, these signals are at sufficient separation and do not affect our experiment.

Victim receiver RX is setup in accordance to our proposed receiver architecture using three crystal locked USRP units Rx0, Rx1 and Rx2 as seen in Fig. 3. The victim antenna is placed 3m from the out-of-band jammers A and B to ensure that they do not overload the receiver front-ends. To demonstrate the performance of the receiver system a narrow-band 12.5 kHz QPSK modulated signal is used for both the desired and jammer signals. The symbol rate is 7.8125 ksymbols/s and filtered with a Nyquist filter with 50% excess bandwidth. Fig. 13 shows the constellation of the desired signal and a 0.5MHz baseband spectrum received at Rx0.

Fig. 13(a) shows the reception of the desired signal at Rx0 without any jammers and interference. The receiver is operated at low IF to avoid any DC offset issues. The low-powered transmitter for the desired signal is mounted in an adjacent room. The scatter plot on the left hand side shows the four QPSK constellation points of the received desired signal at a signal-to-noise ratio (SNR) of about 38dB.

Fig. 13(b) shows the spectrum at Rx0 with the out-of-band colocated jammers turned on. The reverse IM3 product from jammer A falls directly on the desired signal frequency (1367MHz) and completely masks the signal causing major interference. The constellations have an SIR=2dB and are

unrecognizable as a result of interference.

Fig. 13(c) shows the spectrum after DSP correction. The inset compares the spectrum (black) of the DSP corrected signal with the spectrum (blue) of the IM3 distorted signal. Error vector magnitude measurements on the constellation diagrams indicate that the IM3 distortion has been canceled by 16dB, leaving the desired signal with a SIR of about 18dB. The DSP is implemented in MATLAB in accordance to our simulation settings with $OSR = 64$, $N = 4096$ and $M = 2N$. As in Fig. 3, the DSP takes inputs from Rx1 and Rx2, synthesizes a copy of the IM3 and removes it from the primary reception at Rx0. The 18dB SIR achieved is in close agreement to the 20dB output SIR achieved in our simulations (Fig. 4).

Fig. 14(a) and (b) show the baseband frequency spectrums on Rx1 and Rx2 respectively. Rx1 receives the 922MHz jammer A at a frequency offset of 55kHz and Rx2 receives

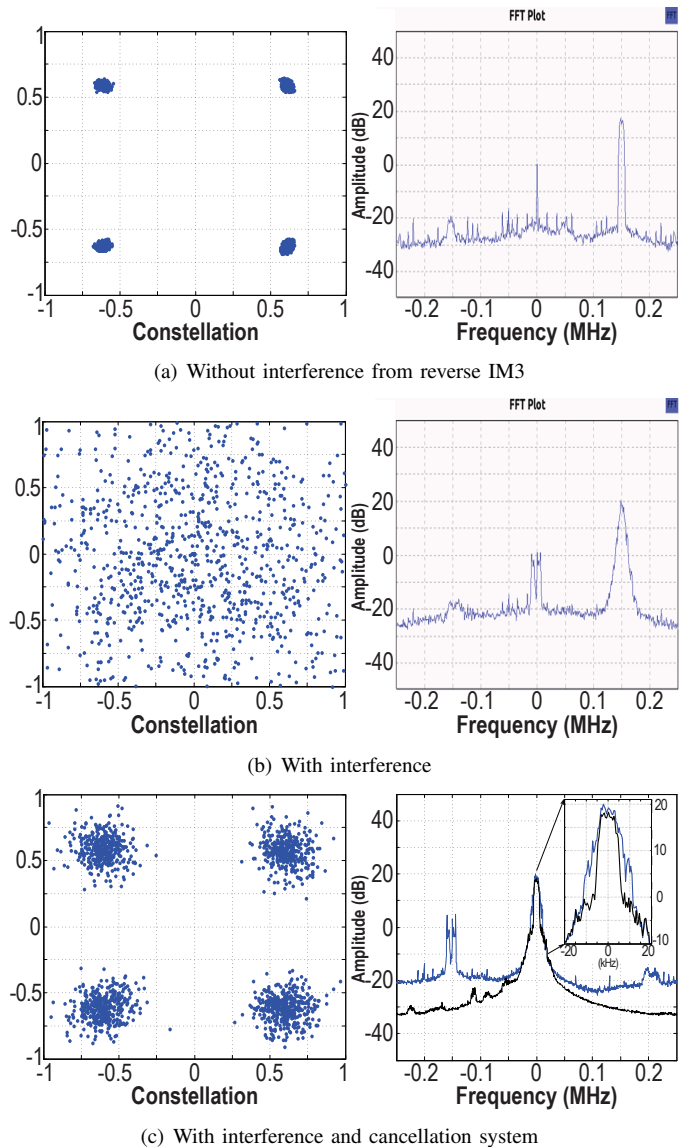


Fig. 13. Experiment results. Signal constellation scatter plots (LHS) and frequency spectrum plots (RHS). The spectrum plots show relative scales with 20dB representing -75dBm.

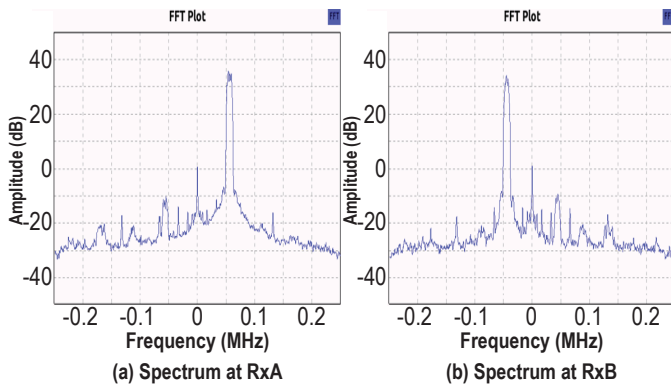


Fig. 14. Frequency spectrum of the jammers.

the 477MHz jammer B at a frequency offset -45kHz . The RF gain on the front-ends are attenuated such that the jammers are within the receiver's dynamic range. Appendix C shows the auxiliary receiver's dynamic range requirements are modest and related to the amount of cancellation required. It should be noted that the jamming signals are significantly larger than the reverse IM3 product (approx. 40-50dB as seen in Fig. 12). If receiver distortion occurs, there is plenty of scope for attenuating the jammers without affecting the quality of the synthesized IM3 estimate \hat{u} .

Fig. 15 shows \hat{f}_k^{Fine} 's fine frequency tracking of the aggregated local oscillator drifts. As estimated, the coarse frequency correction module has reduced the frequency offset to about 0.25 bins ($0.25f_s/N$ Hz). The ripples seen in the figure are primarily due to $\text{RMSE}(\hat{f}_k^{Fine})$ caused by the interference effect of the desired signal in the fine frequency estimation algorithm.

We now consider practical aspects of fielding such a solution. The implementation penalty is dominated by the cost and power consumption associated with the additional receiver chains and their ADCs. Multiple receiver chains on a single integrated circuit are becoming available because of diversity and MIMO requirements in the new standards. The cost and energy consumption continues to drop. An approximate power budget would allow 0.2W per receiver chain [30]. The traditional transmit side solution of filters and isolators involve bulky high power components with insertion loss and often poor frequency agility. A 20W transmitter with two isolators has an additional 1dB insertion loss [31], which represents a dissipation loss of 5W, clearly more than the receiver side solution proposed here.

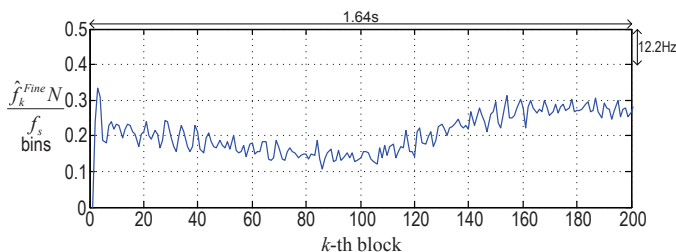


Fig. 15. Fine frequency tracking by \hat{f}_k^{Fine} . $f_s=0.5\text{Msamples/s}$, $N=4096$.

VI. CONCLUSION

Reverse IM products, signal harmonics and other distortions may fall on the desired receive channel of a colocated receiver and cause interference. The paper describes a postdistortion cancellation system for the victim receiver. A distortion regeneration circuit is used to synthesize an estimate of the reverse IM from the jamming signals. This is then used to mitigate (cancel) the distortion on the desired signal. The scheme is flexible and can be used to cancel not only a single reverse IM product but also multiple distortion products, jammer harmonics and any form of distortion where the constituent jamming signals are available. This includes IM products generated within the desired receiver itself. Each different product requires its own generating function and frequency offset correction. The subtraction is done sequentially with the strongest distortion component subtracted first (Fig. 1). The scheme does not need to know the desired signal, s , whose amplitude and phase remains unaffected by the algorithm. As such, signal processing algorithms associated with multiple antenna receivers will not be affected by the canceling. Note, the non-linear polynomial function and frequency offset correction can be a common circuit, but separate gain-phase corrections are required for each receiver chain.

A multi-front-end receiver architecture was used to ensure tracking of out-of-band jammers without the need for extremely high sampling frequencies. This can lead to frequency offsets between the estimate and the reverse IM3 product. The proposed scheme uses a two stage frequency offset correction technique, an FFT for coarse correction and signal correlation for fine frequency tracking. A differential feedback tracking scheme was also devised to track frequency drifts beyond the coarse correction capability. The scheme uses Bussgang's minimum mean squared error formula to correct the estimate's amplitude and phase.

Mathematical analysis and simulations were used to comprehensively characterize the system. The results were then validated in hardware. It was shown that the desired signal acts as noise to the correlator outputs controlling the frequency offset correction and gain phase correction coefficient. To counter this, averaging and increased FFT sizes were necessary.

The output SIR (SIR_o) was shown to be dependent on the equivalent number of uncorrelated samples (N_s) in the averaging block. The maximum SIR improvement possible was shown to be $(N_s - SIR_y)\text{dB}$. Therefore, it is recommended to switch OFF the canceling circuit when $SIR_y < N_s$.

The paper demonstrated a working prototype of the postdistortion cancellation system. Jammers at frequencies 477MHz and 922MHz caused a reverse IM3 product at 1367MHz which is within the GPS³ satellite band. The cancellation algorithm achieved an 18dB output SIR that is in close agreement with the simulation and analytical results. The input SIR was 2dB indicating a 16dB reduction in the reverse IM3 distortion. Had the input SIR been worse, the cancellation would have been correspondingly higher. Table I summarizes related work in distortion cancellation.

³GPS signals are very low level and are particularly sensitive to noise and distortion.

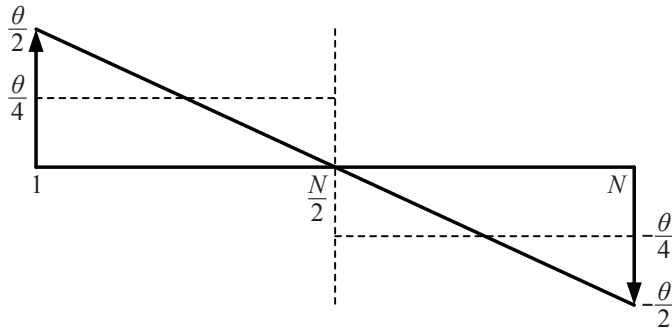


Fig. 16. Linear phase $\theta(= 2\pi f^{Fine} N/f_s)$ across a block.

APPENDIX A THE MODULATION PARAMETER FACTOR η

The variance of the signal ϕ'_k from the correlation of \hat{u}''_k with s_k (the desired signal component in \mathbf{y}_k) is obtained by calculating the power spectrum $P(f)$ of the signal ($s_k \hat{u}''_k$) and then multiplying it with the power frequency response of the averaging function. An N -point averaging filter has a low pass frequency response, with an effective power bandwidth of f_s/N (where f_s is the sampling frequency). We make an approximate solution for the case where all signals have the same bandwidth of f_s/OSR and a rectangular spectral shape. If the desired signal s_k with spectrum $S(f)$ was passed through the averaging filter, its variance would be reduced by $\eta N/OSR$, where $\eta = 1$.

The spectrum $P(f)$ is a convolution of $S(f)$ with the spectrum $\hat{U}(f)$ (of the IM3 distortion signal \hat{u}''_k), which itself is a triple convolution of the spectrums $A(f)$, $A(f)$ and $B(f)$ (of the fundamental jammer signals a and b). i.e. $P(f) = S(f) * \hat{U}(f) = S(f) * A(f) * A(f) * B(f)$. There are 4 convolved terms. We note that the convolution of two unit rectangular signals (power spectral density=1, bandwidth=1) is triangular in shape (magnitude=1, bandwidth=2), and the convolution of two triangles give a signal with a magnitude spectrum of $2/3$ at the center of the band (at DC). Since N is large, the averaging filter bandwidth is very small and we assume a constant spectrum of $P(0)$ over its bandwidth. The variance is, therefore, reduced by $(9/4)N/OSR$, giving $\eta = 9/4$. Of course, the magnitude of $A(f)$ and $B(f)$ also has an effect on the variance, but this is accounted for by the normalization when ϕ'_k goes to $\hat{\rho}_k$.

APPENDIX B THE VARIANCE OF \hat{f}_k^{Fine} DUE TO FREQUENCY OFFSET

The linear phase shift of θ across the block in the second term in (52) produces an orthogonal error ϵ_k in ϕ_k , the mean of which is zero. For small θ ,

$$\bar{\epsilon}_k = \frac{1}{N} \sum_1^N \rho \hat{u}_{n,k} \hat{u}_{n,k}^* \left(\frac{\theta}{2} - \frac{\theta n}{N} \right) e^{-j\psi_k} = 0. \quad (58)$$

We now split the summation into 2 parts (Fig. 16). The mean for the first and second $N/2$ samples is $\bar{\epsilon}_{k,1} = \left(\frac{\theta}{4}\right) \rho \sigma_u^2 e^{-j\psi_k}$ and $\bar{\epsilon}_{k,2} = \left(-\frac{\theta}{4}\right) \rho \sigma_u^2 e^{-j\psi_k}$ respectively. The variance for both

halves are,

$$\begin{aligned} \sigma_{\epsilon_{k,1}}^2 = \sigma_{\epsilon_{k,2}}^2 &= \frac{2}{N} \sum_1^{N/2} \rho^2 \sigma_u^4 \left\{ \left(\frac{\theta}{2} - \frac{\theta n}{N} \right) - \left(\frac{\theta}{4} \right) \right\}^2 \\ &= \frac{\theta^2}{48} \rho^2 \sigma_u^4. \end{aligned} \quad (59)$$

When we average over all N samples the mean goes to zero and the variance becomes $\sigma_{\epsilon_k}^2 = \frac{\theta^2}{48N_s} \rho^2 \sigma_u^4$. We then substitute for θ as per (46), and change back to a phase error $\sigma_{\angle \phi_k}^2 = \tan^{-1} \left(\sigma_{\epsilon_k}^2 / |\bar{\phi}_k|^2 \right)$ by using the small angle approximation. The phase error variance is doubled after the subtraction of (33) to give \hat{f}_k^{Fine} . Thus, the variance of \hat{f}_k^{Fine} due to the second term in (52) becomes

$$\sigma_{\hat{f}_{k,2}^{Fine}}^2 = \frac{(f^{Fine})^2}{24N_s}. \quad (60)$$

APPENDIX C AUXILIARY RECEIVER DYNAMIC RANGE

We show that the maximum level of IM cancellation determines the minimum dynamic range of the auxiliary receivers. If the auxiliary receivers include noise (and other error) terms, n_a and n_b , from receiver Rx1 and Rx2 respectively, then equation (19) becomes:

$$\hat{u} = b^* a^2 + 2b^* a n_a + a^2 n_b^* + O(n^2) \quad (61)$$

where the sub-scripts have been dropped for clearer understanding. The first term is the wanted regenerated distortion term and the second and third terms are the most dominant error terms. The others are much smaller and neglected. Even if there is perfect cancellation of the distortion term in equation (37), these error terms remain and corrupt the desired signal, forming a floor to SIR_o . The maximum cancellation C_{max} is therefore given by,

$$C_{max} (= SIR_o/SIR_y) = E\{|b^* a^2|^2\} / E\{|2b^* a n_a + a^2 n_b^*|^2\} \quad (62)$$

For example, if we assume $b \sim a$, $n_a \sim n_b$, then $C_{max} = E\{|a|^2\} / 5E\{|n_a|^2\}$ or $C_{max}(\text{dB}) = -7(\text{dB}) + \text{SNR}_a(\text{dB})$. A 30dB maximum cancellation limit would call for auxiliary receiver dynamic ranges of 37dB, leading to ADC resolutions of at least 7 bits provided quantization noise was the dominant error source.

REFERENCES

- [1] K. Allsebrook and C. Ribble, "VHF cosite interference challenges and solutions for the United States Marine Corps' expeditionary fighting vehicle program," in *Proc. IEEE Military Communications Conference*, 2004.
- [2] F. German, K. Annamalai, M. Young, M. C. Miller, "Simulation and Data Management for Cosite Interference Prediction," in *Proc. IEEE International Symposium on Electromagnetic Compatibility*, July 2010.
- [3] I. Demirkiran, D. D. Weiner, A. Drozd and I. Kasperovich, "Knowledge-based Approach to Interference Mitigation for EMC of Transceivers on Unmanned Aircraft," in *Proc. IEEE International Symposium on Electromagnetic Compatibility*, July 2010.
- [4] S. Ahmed and M. Faulkner, "Interference Issues at Co-located Base Stations and an Adaptive Cancellation Solution," in *Proc. Electromagnetic Compatibility Symposium and Exhibition Melbourne*, September 2010.

- [5] J. J. Gavan and M. B. Shulman, "Effects of Desensitization on Mobile Radio System Performance, Part I: Quantitative Analysis," *IEEE Transactions on Vehicular Technology*, vol. VT-33, no. 4, pp. 285-290, November 1984.
- [6] B. Razavi, *RF Microelectronics*, Upper Saddle River, NJ: Prentice Hall, 1998.
- [7] S. Ahmed and M. Faulkner, "Optimized Interference Canceling for Co-located Base Station Transceivers," *IEEE Transactions on Vehicular Technology*, vol. 60, no. 9, pp. 4175 - 4183, November 2011.
- [8] LTE; Evolved Universal Terrestrial Radio Access (E-UTRA); Base Station (BS) Radio Transmission and Reception. *3GPP Technical Specification*. 3GPP TS 36.104 ver. 10.6.0 Release 10. [Online]. Available: http://www.etsi.org/deliver/etsi_ts/136100_136199/136104/10.06_00_60/ts_136104v100600p.pdf
- [9] Netcom Inc. Integrated Filter Power Amplifier. Cosite Interference Solution for FDMA Applications. NETCOM Model 3262. *Data Sheet*. [Online]. Available: <http://www.netcominc.com/downloads/Cutsheet-3262-IFPA-4-19-10-DH.pdf>
- [10] Alain Roussel, Charles W. T. Nicholls, and Jim S. Wight, "Frequency Agile RF Feedforward Noise Cancellation System," in *Proc. IEEE Radio and Wireless Symposium*, 2008.
- [11] A. Katz, D. McGee, C. Brinton and J. Qiu, "Sensitivity and Mitigation of Reverse IMD in Power Amplifiers," in *Proc. IEEE Topical Conference on Power Amplifiers for Wireless and Radio Applications (PAWR)*, January 2011.
- [12] T. Nojima, T. Konno, "Cuber Predistortion Linearizer for Relay Equipment in 800 MHz Band Land Mobile Telephone System," *IEEE Transactions on Vehicular Technology*, vol. 34, no. 4, pp. 169-177, November 1985.
- [13] H. Matsubara, K. Ishihara, N. Miyadai, T. Nojima, "A Novel 3rd-and-5th-Order Predistortion Circuit for 2 GHz Band W-CDMA Amplifier," in *Proc. Asia-Pacific Microwave Conference (APMC)*, pp. 1-4, 11-14 December 2007.
- [14] T. Rahkonen, T. Kankaala, M. Neitola, "A Programmable Analog Polynomial Predistortion Circuit for Linearising Radio Transmitters," in *Proc. 24th European Solid-State Circuits Conference*, pp. 276-279, 22-24 September 1998 .
- [15] K. H. Lim, G. Ahn, S. Jung, H. C. Park, M. S. Kim, J. H. Van, H. Cho, J. H. Jeong, C. S. Park, Y. Yang, "A 60-W Multicarrier WCDMA Power Amplifier Using an RF Predistorter," *IEEE Transactions on Circuits and Systems II: Express Briefs*, vol. 56, no. 4, pp. 265-269, April 2009.
- [16] S. P. Stapleton, F. C. Costescu, "An Adaptive Predistorter for a Power Amplifier Based on Adjacent Channel Emissions," *IEEE Transactions on Vehicular Technology*, vol. 41, no. 1, pp. 49-56, 1992.
- [17] G. Baudoin, P. Jardin, "Adaptive Polynomial Pre-distortion for Linearization of Power Amplifiers in Wireless Communications and WLAN," in *Proc. International Conference on Trends in Communications (EUROCON)*, pp. 157-160, 4-7 July, 2001.
- [18] M. Faulkner, "DC Offset and IM2 Removal in Direct Conversion Receivers," *IEE Proc. Communication*, vol. 149, no. 3, pp. 179-184, June 2002.
- [19] E. A. Keehr, A. Hajimiri, "Analysis of Internally Bandlimited Multi-stage Cubic-Term Generators for RF Receivers," *IEEE Transactions on Circuits and Systems I: Regular Papers*, vol. 56, no. 8, pp. 1758-1771, August 2009.
- [20] E. A. Keehr, A. Hajimiri, "Successive Regeneration and Adaptive Cancellation of Higher Order Intermodulation Products in RF Receivers," *IEEE Transactions on Microwave Theory and Techniques*, vol. 59, no. 5, pp. 1379 - 1396, March 2011.
- [21] M. Valkama, A. S. H. Ghadam, L. Anttila, M. Renfors, "Advanced Digital Signal Processing Techniques for Compensation of Nonlinear Distortion in Wideband Multicarrier Radio Receivers," *IEEE Transactions on Microwave Theory and Techniques*, vol. 54, no. 6, pp. 2356 - 2366, June 2006.
- [22] Ettus Research LLC. Universal Software Radio Peripheral. *Product Details*. [Online]. Available: <https://www.ettus.com/product/details/USRP-PKG>
- [23] Ettus Research LLC. WBX 50-2200MHz Rx/Tx. *Product Details*. [Online]. Available: <https://www.ettus.com/product/details/WBX>
- [24] J. Armstrong, "Analysis of New and Existing Methods of Reducing Intercarrier Interference Due to Carrier Frequency Offset in OFDM," *IEEE Transactions on Communications*, vol. 47, no. 3, pp. 365-369, March 1999.
- [25] B. Ai, Z. Yang, C. Pan, J. Ge, Y. Wang, Z. Lu, "On the Synchronization Techniques for Wireless OFDM Systems," *IEEE Transactions on Broadcasting*, vol. 52, no. 2, pp. 236 - 244, June 2006.
- [26] Y. Yao, G. B. Giannakis, "Blind Carrier Frequency Offset Estimation in SISO, MIMO, and Multiuser OFDM Systems," *IEEE Transactions on Communications*, vol. 53, no. 1, pp. 173-183, January 2005.
- [27] M. F. Sun, J. Y. Yu, T. Y. Hsu, "Estimation of Carrier Frequency Offset With I/Q Mismatch Using Pseudo-Offset Injection in OFDM Systems," *IEEE Transactions on Circuits and Systems I: Regular Papers*, vol. 55, no. 3, pp. 943-952, April 2008.
- [28] J. J. Bussgang, "Crosscorrelation Functions of Amplitude Distorted Gaussian Signals," Research Laboratory of Electronics, M. I. T., Cambridge, MA, Technical Report no. 216, March 1952.
- [29] Mini-Circuits. ZHL-42W Amplifier. *Data Sheet*. [Online]. Available: <http://www.minicircuits.com/pdfs/ZHL-42W.pdf>
- [30] Maxim Integrated Products. WCDMA/HSPA Band I RF-to-Bits Femto-Basestation Radio Receiver. MAX2547. *Product Details*. [Online]. Available: <http://www.maxim-ic.com/datasheet/index.mvp/id/5435>
- [31] Fairview Microwave Inc. Coaxial Isolators and Circulators. [Online]. Available: http://www.fairviewmicrowave.com/coaxial_isolators_sma.htm



Shabbir Ahmed Biography text here.



Mike Faulkner Biography text here.